iScience

CellPress
OPEN ACCESS

Article

Atmospheric deposition contributed mostly to organophosphorus flame retardant entering into the Bohai Sea, China

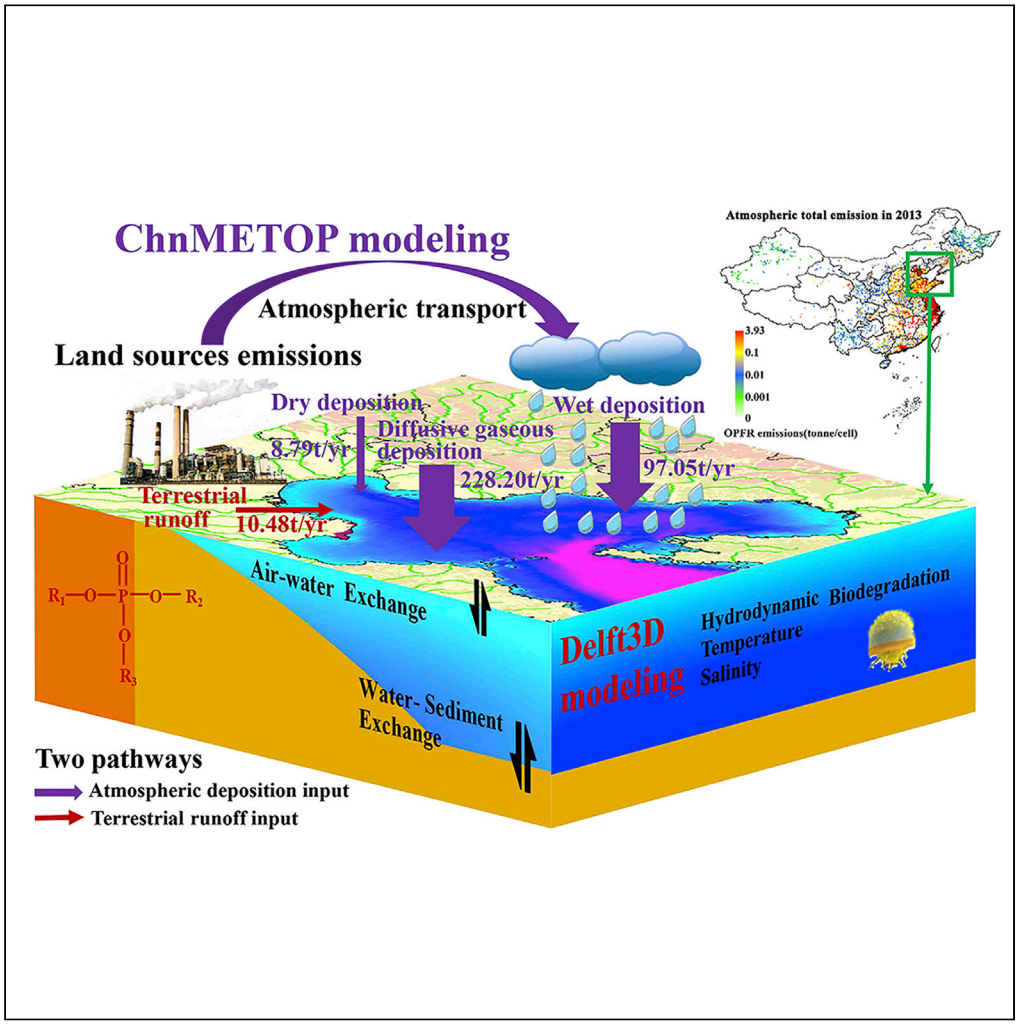

Jian He, Haibo Ma, Zhanxiang Wang, ..., Tao Huang, Hong Gao, Jianmin Ma

honggao@lzu.edu.cn

Highlights

Net OPFR flux input into the BS from two passways were quantified

OPFR input into the BS was dominated by atmospheric loadings

OPFR entering into the BS from terrestrial runoff was negligible

OPFR pollution control in the BS should focus on its air emission reduction

He et al., iScience 26, 105706
January 20, 2023
https://doi.org/10.1016/j.isci.2022.105706

iScience

CellPress
OPEN ACCESS

Article

Atmospheric deposition contributed mostly to organophosphorus flame retardant entering into the Bohai Sea, China

Jian He,[1] Haibo Ma,[1] Zhanxiang Wang,[1] Hongyu Li,[1] Haoyue Fan,[1] Lulu Lian,[1] Min Wu,[1] Shijie Song,[1] Jiabao Zhang,[1] Tao Huang,[1] Hong Gao,[1,3,*] and Jianmin Ma[1,2]

SUMMARY

Atmospheric emission sources of persistent organic pollutants (POPs) in China's eastern seaboard regions cause heavy POP contamination in the Bohai Sea (BS), China. Because many rivers are emptying into the BS, terrestrial runoff has been considered a dominant pathway of POPs onto the BS. Here, we explored the contribution of atmospheric transport and terrestrial runoff to organophosphorus flame retardants (OPFRs) to the BS by using an atmospheric transport model and a terrestrial runoff model. We examined the sensitivity and response of OPFR in the BS seawater to its atmospheric transport, deposition, and riverine discharge via terrestrial runoff. Both terrestrial runoff and atmospheric transport model simulations reveal that the atmospheric transport and deposition, including dry, wet, and diffusive gaseous deposition, dominate OPFR input into the BS. The total OPFR fluxes entering the BS via the atmospheric pathway and riverine input were 70.4 and 2.8 t/yr in 2013, respectively.

INTRODUCTION

Proximate to one of the most industrialized and polluted regions in Northern China (Figure S1), the Bohai Sea (BS) has been one of the most polluted areas by POPs in the world.[1] The semi-enclosed terrain makes the water exchange between the BS and the open ocean relatively slow, worsening the marine environmental pollution in the BS.[2] As one of the most important fisheries in China, the BS provides a significantly large amount of seafood to peripheral cities and unique sea transportation and harbors.[3] In light of this, the toxic pollution in the BS ecosystem has been a significant concern in the scientific community and government agencies for decades. Extensive investigations have been carried out to elucidate the source-receptor relationships and environmental cycling of POPs and heavy metals in the BS. Many of these studies suggested that rivers were the major sources/pathways of terrestrial pollutants to the BS marine environment, which discharge industrial and municipal wastewater from the surrounding cities and industries into the coastal waters.[4,5] A few studies argued that atmospheric deposition likely played a more important role in toxic contaminants entering the BS seawaters than surface runoff.[6]

To fill knowledge gaps, the present study adopted a novel model framework to explore quantitatively the relative contributions of these two pathways, namely, the atmospheric deposition and surface runoff, to the BS marine environmental pollution. We selected organophosphorus flame retardants (OPFRs) as target toxic chemicals. Given that OPFRs are not chemically bonded with the final product and most congeners are volatile, allows for their easy release into the environment during production or from the products to which they are added through abrasion, volatilization, and leaching and recycling processes.[7] As a result, OPFRs have been detected widely in different environmental matrices and distributed globally,[8] including the pristine polar region and deep seas. The widespread occurrence of OPFRs in the environment has posed risks to humans and terrestrial and aquatic ecological systems.[9] Numerous studies have been conducted to assess OPFR bioaccumulation in human exposure, terrestrial food webs, and marine.[10] Limited epidemiologic studies, including developmental toxicity, carcinogenicity, low birth weight, neurotoxicity, endocrine disruption, and reproductive toxicity, have confirmed their adverse effects on human health.[8,11]

China produces an enormous amount of OPFRs globally and has the highest global market share. He et al.[2] reported that the annual OPFRs emissions in China increased from approximately 670 t/yr in 2014 to 1000 t/yr

[1]Key Laboratory for Environmental Pollution Prediction and Control, Gansu Province, College of Earth and Environmental Sciences, Lanzhou University, Lanzhou 730000, P. R. China

[2]Laboratory for Earth Surface Processes, College of Urban and Environmental Sciences, Peking University, Beijing 100871, P. R. China

[3]Lead contact

*Correspondence: honggao@lzu.edu.cn

https://doi.org/10.1016/j.isci.2022.105706

in 2018. Because the use of OPFRs in China has not been regulated, strong atmospheric emission and subsequent deposition and less-treated OPFR-containing domestic sewage and industrial wastewater would form two pathways, one from the air and the other from the surface runoff, contributing to OPFR contamination in seawater.[5,12–14] To assess OPFRs input into the seawater from these two pathways, extensive field sampling studies of OPFRs have been conducted.[4,15–18] Because of the lack of stable power sources and technicians as well as high cost, the air sampling studies only focused on a few locations in a coastal region. Whereas most field investigations of toxic discharge into the coastal waters via runoff mainly were carried out near river estuaries. These limitations hampered OPFR sampling on a large temporal and spatial scale.[2,19,20]

Liu et al.[21] reported brominated diphenyl ethers 209 (BDE-209) total input of 140 kg/season and decabromodiphenyl ethane (DBDPE) total input of 19 kg/season into the BS via 31 riverine discharge in the summer 2013. The atmospheric deposition fluxes of these two chemicals contributed 21 and 29 kg/season to their abundance in the BS, respectively. The result suggests that the riverine input overwhelmed BDE-209 contamination in the BS, but for DBDPE, atmospheric deposition is a more critical pathway than surface runoff. Although the investigations of OPFR entering the BS via multiple pathways are still lacking, considering that OPFRs also undergo atmospheric transport/deposition and riverine input into surface water bodies via runoff,[7,22–25] and as a flame retardant have almost the same source locations as DEDPE and BDE-209 in China,[2] it is important to clarify the relative contribution of atmospheric deposition and terrestrial runoff of OPFRs to their contamination in the BS. There are still significant knowledge gaps in how OPFRs enter a water body. Field sampling of OPFRs has been conducted in the Pearl River Delta,[26] the BS,[27] and the Yellow Sea.[28] Efforts were also made to estimate air-water diffusive gaseous exchange and deposition above coastal waters.[13,29,30] The "two-way" air-water gaseous exchange fluxes in the coastal area of the BS in Dalian, China, ranged from −7963 ng/m^2/day to 10,744 ng/m^2/day.[29] The recent studies by He et al.[2] and Wang et al.[19] featured perhaps the first investigation to simulate atmospheric transport, deposition, and multi-compartment exchange of OPFRs between different environmental media in the marine environment using novel atmospheric transport and chemistry models.

OPFRs have been extensively used and produced in China.[2] The widespread occurrence of OPFRs in the environment has posed risks to humans and terrestrial and aquatic ecological systems. Located in one of the most industrialized and polluted regions in Northern China, the BS has been one of the most polluted areas by POPs in the world. However, many previous modeling investigations either focused on atmospheric processes or surface runoff processes separately. In particular, because of the lack of reliable and comprehensive atmospheric transport and deposition models, some of previous studies concluded that terrestrial runoff dominated POP fluxes entering the BS. The efforts for integrating or combining atmospheric and surface runoff models to identify their relative significance to the contamination of OPFRs or other POPs in seawater seem still lacking. To fill this knowledge gap, the present study aims to compare and identify the relative contribution of atmospheric transport and deposition as well as discharge by surface runoff to OPFR pollution in the BS via aerodynamic and hydrodynamic modeling. Extensive model simulations are performed to examine OPFR input into the BS through the air pathway formed by atmospheric transport, dry and wet deposition, and air-water exchange, and through surface runoff created by riverine discharge. The result could help relevant government agencies and stakeholders make emission mitigation strategies in the BS ecologic environment control.

RESULTS AND DISCUSSION

Atmospheric deposition fluxes of OPFR

The detailed information of models and data referred to in this section and other sections are provided in STAR Methods, Figures S1–S10, and Tables S1, S2, S3, S4, S5, S6, and S7.

Like other POPs, OPFRs entering a marine environment via the atmospheric pathway follows the release from their emission sources, atmospheric transport and diffusion, and subsequent deposition and diffusive gaseous exchange between air and water. Here, we shall focus only on the deposition processes. Figure 1 displays ChnMETOP modeled annual atmospheric dry, wet, and total (dry + wet) deposition fluxes (mg/m^2/yr) in 2013, obtained by summing modeled annual deposition fluxes at all model grids over the BS. Higher OPFR dry depositions can be found along the coastline, in line with modeled air concentrations because of the proximity of the coastal waters to onshore emission sources.[2] The lower dry deposition fluxes in offshore seawaters are caused not only by increasing distance from onshore OPFR emission sources but also by the smoother sea surface that leads to smaller deposition velocity and dry deposition fluxes.[31]

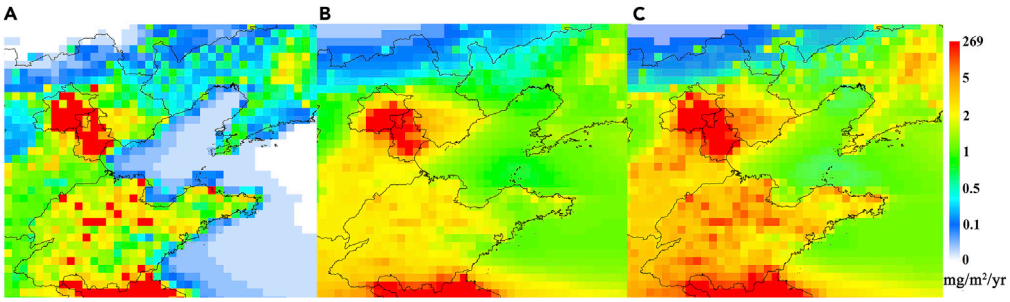

Figure 1. Modeled annual atmospheric deposition to the BS in 2013

(A) Dry deposition (mg/m^2/yr).

(B) Wet deposition (mg/m^2/yr).

(C) Total deposition (dry + wet, mg/m^2/yr).

The OPFR dry deposition into the BS ranged from 0.02 to 1.66 mg/m^2/yr (median: 0.04 mg/m^2/yr), which is higher than that from Northwestern Pacific to the Arctic Ocean ranging from 0 to 0.068 mg/m^2/yr,[22] implying strong OPFR emissions in China. Annual wet deposition fluxes in 2013 over the BS were displayed in Figure 1B. Wet deposition ranged from 0.72 to 3.28 mg/m^2/yr (median: 1.10 mg/m^2/yr). A greater median value of wet deposition than dry deposition suggests that atmospheric loading of OPFRs to the BS was overwhelmed by wet deposition. Both atmospheric concentrations and precipitations contribute to wet loadings of OPFRs to the seawater. The total deposition flux to the BS ranged from 0.77 to 4.85 mg/m^2/yr (median: 1.15 mg/m^2/yr). The deposition flux of OPFRs was relatively higher in the mouth of Bohai Bay. Overall, the total deposition flux to the BS was higher than the Yellow Sea (0.008–0.091 mg/m^2/yr),[16] the North African Mediterranean coastal cities (0.007–0.066 mg/m^2/yr),[32] the South China Sea (0.006 $\pm$ 0.002 mg/m^2/yr),[33] and the North Atlantic and Arctic Oceans (0.0007–0.006 mg/m^2/yr),[13] but similar to the Mediterranean (0.025–0.32 mg/m^2/yr) and the Black Sea (0.109–0.584 mg/m^2/yr).[23]

Gaseous exchange across the air-water interface is a critical process controlling the concentrations and fates of OPFR in a water body.[29,34] As Equation 1 of STAR Methods, the net gas flux in the interface between sea surface water and air mainly depends on the concentration gradient between water and air, Henry's law constant, and the k_{ol} mass transfer coefficient. As aforementioned, negative flux means OPFR deposition from the atmosphere onto the water, whereas positive flux means OPFR volatilization from the water into the air. Our modeling result reveals negative net air-water exchange fluxes of OPFRs from −104310 to −12 ng/m^2/day (median:−607 ng/m^2/day). Given that OPFRs are still used extensively in China,[2] the negative net OPFRs diffusive gas exchange fluxes indicate strong OPFR loadings from the air into the seawater surface or the absorption by the seawater, agreeing, to some extent, with the measured result which reported a downward gaseous deposition flux of Tris(2-chloroisopropyl) phosphate (TCIPP) of −395 $\pm$ 1211 ng/m^2/day in 2013.[29]

OPFR concentrations in seawater

The OPFR levels in the BS seawaters simulated by the Delft3D-WAQ model subject to modeling scenario 1 without atmospheric deposition fluxes are displayed in Figure 2A. He et al.[2] reported that Shandong Province and the Beijing-Tianjin-Hebei region were two of the major land source emission regions of OPFRs in China. Extensive application of OPFRs in industrial and/or domestic sectors and leakage from the OPFR manufacturing can release OPFRs into the atmospheric and terrestrial environment primarily through industrial or municipal wastewater discharge.[7] The Delft3D-WAQ simulated OPFR seawater concentrations in the BS via terrestrial runoff in model scenario 1, without including atmospheric concentration and deposition flux, ranged from 0 to 488 ng/L (median: 0.0037 ng/L) averaged over the BS in 2013, as shown in Figure 2A. Figure 2B displays the Delft3D-WAQ modeled OPFR seawater concentrations across the BS subject to modeling scenario 2, which imposed the fixed mean atmospheric concentration of 2 ng/m^3 and deposition flux of 2000 ng/m^2/day. The simulated OPFR seawater concentration averaged over the entire BS ranged from 0.708 to 2011 ng/L (median: 59.5 ng/L). Compared with the median concentration from model scenario 1, the median concentration from the second model scenario enhanced five orders of magnitude (Figure 2B), suggesting that the atmospheric deposition dominates terrestrial runoff input of OPFR into the BS.

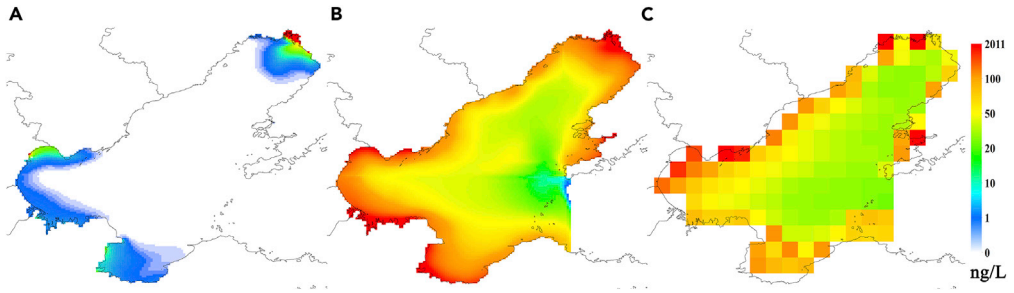

Figure 2. Annually averaged OPFR water concentrations in seawater (ng/L) across the BS simulated

(A) Delft3D-WAQ subject to model scenario 1.

(B) Delft3D-WAQ subject to model scenario 2.

(C) ChnMETOP simulation.

Figure S2 compares Delft3d-WAQ modeled monthly mean OPFR seawater concentrations subject to modeling scenarios 2 and 3 at the selected model grids (38.648°N and 118.895°E) in 2013 by reducing the input atmospheric concentration by 0.2 ng/m^3 and deposition flux (200 ng/m^2/day) in the model scenario 3, which are one order of magnitude higher than the inputs in the model scenario 2. Both modeled OPFR seawater concentrations from scenarios 2 and 3 exhibit identical monthly fluctuations, but the modeled monthly OPFR seawater concentrations are about one order of magnitude higher than the modeled scenario 2 results, suggesting that the seawater concentrations linearly respond to atmospheric concentrations and deposition fluxes in the Delft3D-WAQ model.

Considering significant uncertainty in the selected mean atmospheric concentration and deposition flux input into the Delft3D-WAQ, we further integrate the ChnMETOP to predict OPFR water concentrations in the BS in 2013 through deposition and water-air exchange. Because of the ChnMETOP takes detailed gridded OPFR emissions from different sources across China into account and verified by sampled data and will be elaborated on below,[2] it yielded more reliable OPFR atmospheric concentrations and depositions compared to fixed values taken in the second Delft3D-WAQ scenario run. The ChnMETOP predicted OPFR water concentrations across the BS are illustrated in Figure 2C. Overall, the ChnMETOP and Delft3D-WAQ modeling scenario 2 yield a similar spatial pattern of gridded OPFR water concentrations across the BS. Differing from the Delft3D-WAQ modeled higher water concentrations near the riverine estuaries, the ChnMETOP predicted higher concentrations in the seawater near the coastal waters because of proximity to the major atmospheric emission sources in the BS Rim and prevailing westerly winds (Figure 1).[6] In addition to the source proximity, high OPFRs in coastal waters might also be associated with low salinity.[4,17] The OPFRs concentration decreased offshore with the increase in distance from the shoreline because of atmospheric dispersion and degradation during their journey in the air (Figure 2). For OPFR input from terrestrial runoff, the decreasing concentrations offshore might also be associated with dilution by offshore seawater, absorption of particles, and degradation effects such as hydrolysis, photolysis, and biodegradation during the oceanic transport.[7,35] The ChnMETOP simulated OPFR seawater concentration over the BS ranged from 28.29 ng/L to 955 ng/L (median: 50.65 ng/L). The ChnMETOP modeled median concentration agrees with the Delft3D-WAQ scenario 2 simulation (59.5 ng/L). In addition, the ChnMETOP (Figure 2C) modeled total OPFR water concentration summed over the BS also agrees, to some extent, with sampled total concentration, ranging from 8.12 ng/L to 98.04 ng/L,[17] and comparable to the total OPFR concentration in the German Bight (North Sea), ranging from 5 to 50 ng/L.[4] On the other hand, Delft3D-WAQ simulated OPFR levels from model scenario 2 are in line with measured data in the seawater near coastal cities of the Yellow Sea and the East China Sea, ranging from 91.87 to 1392 ng/L.[36]

Higher OPFR concentrations can be identified in the coastal areas proximate to freshwater runoff input, especially in the estuaries of the Liaohe River, particularly in the mouth of Laizhou Bay, Bohai Bay, and Liaodong Bay as the estuary of the Yellow River, Haihe River, and Liaohe River, the three largest rivers among 36 rivers, emptying into the BS, respectively (Figures 2A and 3). As a result, higher OPFRs in these Bay areas can be attributed to their riverine input. This can be further identified in river estuaries, where OPFR levels were high but dropped sharply away from the coast (Figure 3). Besides the dilution effect of clean water from the high seas, the salting-out effect of organic pollutants might be another factor

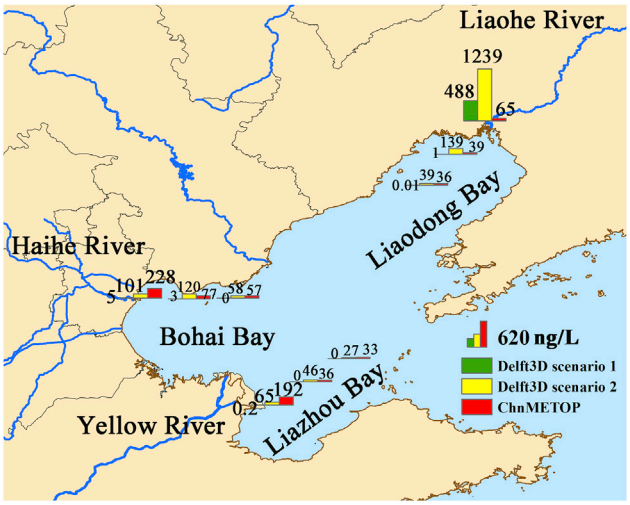

Figure 3. OPFR seawater concentrations in the Laizhou Bay, Bohai Bay, and Liaodong Bay from the estuary (0 , 50, and 100 km) of the Yellow River, Haihe River, and Liaohe River to BS offshore, simulated by Delft3D-WAQ subject to model scenario 1 (Green), scenario 2 (Yellow), and by ChnMETOP (Red), respectively

attributing to the negative correlation between OPFR concentration and water salinity (Figures 3 and S3), which is one of the important reasons for high pollution at river estuaries around the BS.[17] Figures 3, S2, and S3 also show that seawater in the ocean has high salinity and low OPFR levels, and freshwater runoff has low salinity and high pollutant concentrations.

Figure S4 is a correlation diagram between Delft-FLOW molded monthly mean water temperature (Figure S4A) and salinity (Figure S4B) and measured data at the six monitoring sites. The result indicates the excellent agreement between the model simulation and field measurements. Figures S5A and S5B compare the simulated and observed seawater OPFR concentrations at several sampling sites across China, collected from different field campaigns and the literature (Table S1).[17] The result indicates that both ChnMETOP and Delft3D-WAQ scenario 2 simulated seawater concentrations agree well with the measurements at the correlation coefficient $R = 0.79$ ($p < 0.01$) and 0.73 ($p < 0.01$), respectively, although the measured concentrations were slightly higher than the model-predicted concentrations. Table S1 presents the modeled and sampled seawater concentration values at those sampling sites. ChnMETOP predicted more accurate water concentrations, indicating that the atmospheric pathway likely plays a more important role in OPFR contamination in the BS.

Atmospheric deposition versus terrestrial runoff

To further highlight the relative significance of atmospheric and terrestrial runoff pathways for OPFR entering into the BS, we calculated the cumulative OPFR input into the BS by summing all net input at those model grids within the BS water area. Figure 4 compares the total riverine input, net air-water exchange fluxes, and atmospheric deposition of OPFR to the BS in 2013. Among the atmospheric and runoff pathways, terrestrial runoff accounts for OPFR loading of 10.48 t/yr, dry deposition accounts for the OPFR loading of 8.79 t/yr, and wet deposition accounts for the OPFR loading of 97.05 t/yr. Net air-water exchange fluxes contribute to the OPFR loading of 228.20 t/yr, which is over one order of magnitude higher than atmospheric depositions. As a result, the total OPFR loading through the three atmospheric pathways was 334 t/yr, significantly higher than the riverine input. Likewise, the net riverine input in 2013 estimated by the Delft3D-WAQ scenario 1 was merely 2.77 t/yr (Figure 2A), and the net input via the atmospheric deposition and air-water exchange stimulated by the ChnMETOP was 70.40 t/yr for the same year (Figure 2C). Wang et al.[5] estimated the total riverine input of OPFR into BS in 2013 at 16 ± 3.2 t/yr, which is almost one order of magnitude higher than the Delft3D-WAQ modeling result. Little information on OPFR atmospheric deposition to the open water of a marine system is available. Bollmann et al.'s calculation[4] indicates that the OPFR riverine input into the German Bight (North Sea) reached 50 t/yr. Castro-Jimenez et al.[32] have estimated OPFR loadings in the Mediterranean marine ecosystem and indicated that the Mediterranean Sea open water received 13 to 260 t/yr of

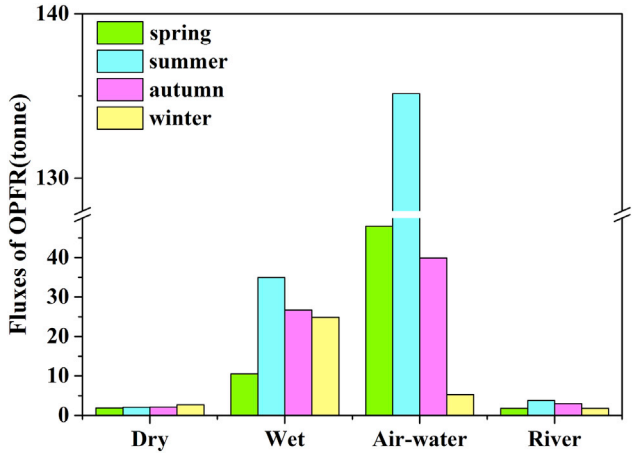

Figure 4. Seasonal accumulate dry deposition (t/period), wet deposition (t/period), air-water exchange fluxes (t/period), and riverine input fluxes (t/period) of OPFRs to the BS in 2013, summed from their respective daily fluxes in each season

OPFRs from the atmosphere.[32] Overall, although terrestrial runoff plays a vital role in the OPFR input into the BS marine environment,[21,37] atmospheric transport and subsequent deposition tend to overwhelm the OPFR loadings to the BS. The result suggests that the atmosphere is a more efficient and faster pathway of toxic chemicals to a marine system, which can carry chemicals from their local, nearby, and remote sources to a receptor under favorable atmospheric circulation systems. In our case, the BS is located to the west and north of major land sources of OPFRs. The chemical from those nearby sources in Shandong and Northern Jiangsu provinces (Figure S6) could be directly carried and diffused to the BS by the Asian summer monsoon (Figure S7A). Whereas in the wintertime, the prevailing westerly winds and winter monsoon system favor easterly transport of OPFRs from Northern Hebei and inland sources to the BS (Figure S7B).

Figure 4 illustrates seasonal accumulate dry deposition, wet deposition, and the net air-water exchange fluxes as well as and terrestrial runoff of OPFRs to the BS in spring (Mar-May), summer (Jun-Aug), autumn (Sep-Nov), and winter (Dec-Feb) in 2013, respectively. The accumulate fluxes were summered from modeled daily fluxes in each season. The dry deposition flux was the highest in winter and lowest in spring. Given that OPFR emissions were not subject to seasonal variation,[2] the seasonal change in the dry deposition flux largely depended on the physicochemical properties of OPFRs and weather conditions.[6] In the wintertime, relatively low temperatures promote the partitioning of OPFRs from air to liquid or solid, and thus the chemicals have a high tendency to be deposited onto seawaters or ice that often occurs in the northern and western BS with very low temperatures. The lower temperatures also extended the residence time of OPFR in the marine and atmospheric environment.[31] In contrast, the largest wet and terrestrial runoff loadings of OPFRs occurred in summer, which was attributed to high precipitations over the BS region during the East Asian summer monsoon season. We also observed largest air-water diffusive gaseous exchange fluxes during the summertime throughout 2013. This is largely attributable to the significantly higher OPFR air concentrations revitalized from the soils and other secondary sources in nearby industries and cities around the BS associated with higher temperatures, which favors solid to gas phase partitioning.

Conclusions

The ChnMETOP and Delft3D simulations were performed to quantitatively assess the relative contributions of atmospheric deposition and riverine discharge via terrestrial runoff to OPFR contamination in the BS environment. The modeling results revealed that the ChnMETOP modeled OPFR levels in the BS seawater ranged from 28.29 ng/L to 955 ng/L (median: 50.65 ng/L), and Delft3D simulated concentrations excluding atmospheric pathway ranged from 0 to 488 ng/L (median: 0.0037 ng/L), respectively. The net riverine input of OPFR into the BS was 2.77 t/yr in 2013, and the total atmospheric pathway (dry + wet + diffusive gaseous deposition) yielded the net OPFR input of 70.40 t/yr, indicating that the atmospheric pathway plays a more important role in the OPFR contamination to the BS. We also assessed the OPFR spatial distribution across the BS simulated by the two models and attributed such distribution to the atmospheric circulation systems

and hydrodynamics in the seawater. The findings of the present study may raise a concern to policymakers regarding the improvement of BS marine environment. In many cases, the sources of riverine and wastewater discharge of toxic chemicals are readily identified and traced because the majority of these sources come from wastewater plants and cities with extensive industrial and human activities, which could be accurately pinpointed. As a result, the riverine runoff discharge could be effectively reduced by shutting down the chemicals' sources linking with the rivers emptying into the BS. For atmospheric transport and deposition, however, even though chemicals' sources could be identified in their atmospheric emission inventory, large uncertainties in the emission inventory, complex atmospheric circulation systems, turbulent activities, and many other gain and loss mechanisms in the atmosphere cause greater difficulties to accurately tag major nearby and remote sources contributing to chemicals' pollution in the marine environment. To effectively mitigate the major emission sources of OPFR and other toxic contaminants and improve the BS marine environment, more efforts need to be made to enhance our understanding of atmospheric pathways and source-receptor relationships.

Limitations of the study

Major limitations come from the uncertainties in emission inventory and multiple dynamic and physical processes in the atmospheric and runoff model. The evaluation of these uncertainties needs extensive field measurement data, which, however, are often not sufficient. Although great efforts have been made to conduct field sampling studies, many of such studies used passive samplers to measure air concentrations. These passive samplers themselves are subject to errors and uncertainties, which causes additional difficulties to modeling results verification. To have more robust model comparison and optimization, synthetic time-series datasets generated from reliable data sources would improve modeling results in future.

STAR★METHODS

Detailed methods are provided in the online version of this paper and include the following:

- KEY RESOURCES TABLE
- RESOURCE AVAILABILITY
  - Lead contact
  - Materials availability
  - Data and code availability
- METHOD DETAILS
  - The Bohai Sea
  - 3D-hydrodynamic and emerging contaminant model
  - Atmospheric transport model
  - Loading estimation
  - Uncertainty and sensitivity analysis of atmospheric deposition
  - Validation of 3D-hydrodynamic model

SUPPLEMENTAL INFORMATION

Supplemental information can be found online at https://doi.org/10.1016/j.isci.2022.105706.

ACKNOWLEDGMENTS

This study was supported by the National Natural Science Foundation of China (grants 41991312, 42177351, U1806207 and 41877507).

AUTHOR CONTRIBUTIONS

H.G. and J.H. designed the study; J.H. performed model simulations; J.H., H.M., Z.W., H.L., H.F., L.L., M.W., S.S., and J.Z. collected the data; J.H., H.G., J.M., and T.H. participated in the acquisition, analysis, and interpretation of data.

DECLARATION OF INTERESTS

The authors declare no competing interests.

Received: July 18, 2022
Revised: November 5, 2022
Accepted: November 28, 2022
Published: January 20, 2023

REFERENCES

1. Li, X., Yan, G., Wang, Y., and Pan, Y. (2014). Emerging persistent organic pollutants in Chinese bohai sea and its coastal regions. Sci. World J. *1–10*.

2. He, J., Wang, Z., Zhao, L., Ma, H., Huang, J., Li, H., Mao, X., Huang, T., Gao, H., and Ma, J. (2021). Gridded emission inventory of organophosphorus flame retardants in China and inventory validation. Environ. Pollut. *290*, 118071.

3. Gao, X., Zhou, F., and Chen, C.T.A. (2014). Pollution status of the Bohai Sea: an overview of the environmental quality assessment related trace metals. Environ. Int. *62*, 12–30.

4. Bollmann, U.E., Möller, A., Xie, Z., Ebinghaus, R., and Einax, J.W. (2012). Occurrence and fate of organophosphorus flame retardants and plasticizers in coastal and marine surface waters. Water Res. *46*, 531–538.

5. Wang, R., Tang, J., Xie, Z., Mi, W., Chen, Y., Wolschke, H., Tian, C., Pan, X., Luo, Y., and Ebinghaus, R. (2015). Occurrence and spatial distribution of organophosphate ester flame retardants and plasticizers in 40 rivers draining into the BS, north China. Environ. Pollut. *198*, 172–178.

6. Jiang, W., Huang, T., Chen, H., Lian, L., Liang, X., Jia, C., Gao, H., Mao, X., Zhao, Y., and Ma, J. (2018). Contamination of short-chain chlorinated paraffins to the biotic and abiotic environments in the Bohai Sea. Environ. Pollut. *233*, 114–124.

7. Wei, G.L., Li, D.Q., Zhuo, M.N., Liao, Y.S., Xie, Z.Y., Guo, T.L., Li, J.J., Zhang, S.Y., and Liang, Z.Q. (2015). Organophosphorus flame retardants and plasticizers: sources, occurrence, toxicity and human exposure. Environ. Pollut. *196*, 29–46.

8. Yang, J., Zhao, Y., Li, M., Du, M., Li, X., and Li, Y. (2019). A review of a class of emerging contaminants: the classification, distribution, intensity of consumption, synthesis routes, environmental effects and expectation of pollution abatement to organophosphate flame retardants (OPFRs). Int. J. Mol. Sci. *20*, 2874.

9. Mihajlović, I., and Fries, E. (2012). Atmospheric deposition of chlorinated organophosphate flame retardants (OFR) onto soils. Atmos. Environ. *56*, 177–183.

10. Zhao, H., Zhao, F., Liu, J., Zhang, S., Mu, D., An, L., Wan, Y., and Hu, J. (2018). Trophic transfer of organophosphorus flame retardants in a lake food web. Environ. Pollut. *242*, 1887–1893.

11. Xiang, P., Liu, R.Y., Li, C., Gao, P., Cui, X.Y., and Ma, L.Q. (2017). Effects of organophosphorus flame retardant TDCPP on normal human corneal epithelial cells: implications for human health. Environ. Pollut. *230*, 22–30.

12. Ya, M., Wu, Y., Wu, S., Li, Y., Mu, J., Fang, C., Yan, J., Zhao, Y., Qian, R., Lin, X., and Wang, X. (2019). Impacts of seasonal variation on organochlorine pesticides in the east China sea and northern south China sea. Environ. Sci. Technol. *53*, 13088–13097.

13. Li, J., Xie, Z., Mi, W., Lai, S., Tian, C., Emeis, K.C., and Ebinghaus, R. (2017). Organophosphate esters in air, snow and seawater in the North Atlantic and the arctic. Environ. Sci. Technol. *51*, 6887–6896.

14. Morales, L., Dachs, J., Fernández-Pinos, M.C., Berrojalbiz, N., Mompean, C., González-Gaya, B., Jiménez, B., Bode, A., Ábalos, M., and Abad, E. (2015). Oceanic sink and biogeochemical controls on the accumulation of polychlorinated dibenzo-p-dioxins, dibenzofurans, and biphenyls in plankton. Environ. Sci. Technol. *49*, 13853–13861.

15. Bekele, T.G., Zhao, H., Wang, Q., and Chen, J. (2019). Bioaccumulation and trophic transfer of emerging organophosphate flame retardants in the marine food webs of laizhou bay, north China. Environ. Sci. Technol. *53*, 13417–13426.

16. Li, J., Tang, J., Mi, W., Tian, C., Emeis, K.C., Ebinghaus, R., and Xie, Z. (2018). Spatial distribution and seasonal variation of organophosphate esters in air above the Bohai and Yellow Seas, China. Environ. Sci. Technol. *52*, 89–97.

17. Zhong, M., Tang, J., Mi, L., Li, F., Wang, R., Huang, G., and Wu, H. (2017). Occurrence and spatial distribution of organophosphorus flame retardants and plasticizers in the bohai and yellow seas, China. Mar. Pollut. Bull. *121*, 331–338.

18. Möller, A., Sturm, R., Xie, Z., Cai, M., He, J., and Ebinghaus, R. (2012). Organophosphorus flame retardants and plasticizers in airborne particles over the northern Pacific and Indian Ocean toward the polar regions: evidence for global occurrence. Environ. Sci. Technol. *46*, 3127–3134.

19. Wang, L., Huang, Y., Zhang, X., Liu, X., Chen, K., Jian, X., Liu, J., Gao, H., Zhugu, R., and Ma, J. (2022). Mesoscale cycling of organophosphorus flame retardants (OPFRs) in the Bohai Sea and Yellow Sea biotic and abiotic environment: a WRF-CMAQ modeling. Environ. Pollut. *298*, 118859.

20. O'Driscoll, K., Mayer, B., Ilyina, T., and Pohlmann, T. (2013). Modelling the cycling of persistent organic pollutants (POPs) in the North Sea system: fluxes, loading, seasonality, trends. J. Mar. Syst. *111–112*, 69–82.

21. Liu, L., Zhen, X., Wang, X., Li, Y., Sun, X., and Tang, J. (2020). Legacy and novel halogenated flame retardants in seawater and atmosphere of the BS: spatial trends, seasonal variations, and influencing factors. Water Res. *184*, 116117.

22. Na, G., Hou, C., Li, R., Shi, Y., Gao, H., Jin, S., Gao, Y., Jiao, L., and Cai, Y. (2020). Occurrence, distribution, air-seawater exchange and atmospheric deposition of organophosphate esters (opes) from the northwestern pacific to the arctic ocean. Mar. Pollut. Bull. *157*, 111243.

23. Castro-Jiménez, J., Berrojalbiz, N., Pizarro, M., and Dachs, J. (2014). Organophosphate ester (OPE) flame retardants and plasticizers in the Open Mediterranean and Black Seas atmosphere. Environ. Sci. Technol. *48*, 3203–3209.

24. Ma, Y., Xie, Z., Lohmann, R., Mi, W., and Gao, G. (2017). Organophosphate ester flame retardants and plasticizers in ocean sediments from the North pacific to the Arctic Ocean. Environ. Sci. Technol. *51*, 3809–3815.

25. Pantelaki, I., and Voutsa, D. (2019). Organophosphate flame retardants (OPFRs): a review on analytical methods and occurrence in wastewater and aquatic environment. Sci. Total Environ. *649*, 247–263.

26. Liu, Y.E., Luo, X.J., Huang, L.Q., Zeng, Y.H., and Mai, B.X. (2019). Organophosphorus flame retardants in fish from rivers in the pearl river delta, south China. Sci. Total Environ. *663*, 125–132.

27. Qi, Y., He, Z., Yuan, J., Ma, X., Du, J., Yao, Z., and Wang, W. (2021). Comprehensive evaluation of organophosphate ester contamination in surface water and sediment of the BS, China. Mar. Pollut. Bull. *163*, 112013.

28. Mi, L., Xie, Z., Zhao, Z., Zhong, M., Mi, W., Ebinghaus, R., and Tang, J. (2019). Occurrence and spatial distribution of phthalate esters in sediments of the bohai and yellow seas. Sci. Total Environ. *653*, 792–800.

29. Wang, Y., Wu, X., Zhang, Q., Zhao, H., Hou, M., Xie, Q., and Chen, J. (2018). Occurrence, distribution, and air-water exchange of organophosphorus flame retardants in a typical coastal area of China. Chemosphere *211*, 335–344.

30. McDonough, C.A., Puggioni, G., Helm, P.A., Muir, D., and Lohmann, R. (2016). Spatial distribution and air-water exchange of organic flame retardants in the Lower Great Lakes. Environ. Sci. Technol. *50*, 9133–9141.

31. Ma, J., Daggupaty, S., Harner, T., Blanchard, P., and Waite, D. (2004). Impacts of lindane usage in the Canadian prairies on the Great Lakes ecosystem. 2. Modeled dry, wet depositions and net gas exchange fluxes, and loadings to the Great Lakes. Environ. Sci. Technol. *38*, 984–990.

32. Castro-Jiménez, J., and Sempéré, R. (2018). Atmospheric particle-bound organophosphate ester flame retardants and plasticizers in a North African Mediterranean coastal city (Bizerte, Tunisia). Sci. Total Environ. *642*, 383–393.

33. Lai, S., Xie, Z., Song, T., Tang, J., Zhang, Y., Mi, W., Peng, J., Zhao, Y., Zou, S., and Ebinghaus, R. (2015). Occurrence and dry deposition of organophosphate esters in atmospheric particles over the northern South China Sea. Chemosphere *127*, 195–200.

34. Ruge, Z., Muir, D., Helm, P., and Lohmann, R. (2015). Concentrations, trends, and air-water exchange of PAHs and PBDEs derived from passive samplers in Lake Superior in 2011. Environ. Sci. Technol. *49*, 13777–13786.

35. Zhen, X., Li, Y., Tang, J., Wang, X., Liu, L., Zhong, M., and Tian, C. (2021). Decabromodiphenyl ether versus decabromodiphenyl ethane: source, fate, and influencing factors in a coastal sea nearing source region. Environ. Sci. Technol. *55*, 7376–7385.

36. Hu, M., Li, J., Zhang, B., Cui, Q., Wei, S., and Yu, H. (2014). Regional distribution of halogenated organophosphate flame retardants in seawater samples from three coastal cities in China. Mar. Pollut. Bull. *86*, 569–574.

37. Bacaloni, A., Cucci, F., Guarino, C., Nazzari, M., Samperi, R., and Laganà, A. (2008). Occurrence of organophosphorus flame retardant and plasticizers in three volcanic lakes of Central Italy. Environ. Sci. Technol. *42*, 1898–1903.

38. Hydraulics, D. (2020a). Delft3D- Water Quality User Manual (Delft, the Netherlands).

39. USEPA (2004). EPI suite™-estimation program interface. https://www.epa.gov/tsca-screening-tools/epi-suitetm-estimation-program-interface.

40. Scheringer, M. (2011). Procedure for estimating chemical properties and chemical concentrations in different media of an environmental fate model. http://www.ipcp.ethz.ch/Armenia/Using_EpiSuite_and_Box_Models.pdf.

41. Ma, J., Daggupaty, S., Harner, T., and Li, Y. (2003). Impacts of lindane usage in the Canadian prairies on the Great Lakes ecosystem. 1. Coupled atmospheric transport model and modeled concentrations in air and soil. Environ. Sci. Technol. *37*, 3774–3781.

42. Ma, J., Venkatesh, S., Li, Y.F., and Daggupaty, S. (2005). Tracking toxaphene in the North American great lakes basin. 1. Impact of toxaphene residues in United States soils. Environ. Sci. Technol. *39*, 8123–8131.

43. Huang, T., Ling, Z., Ma, J., Macdonald, R.W., Gao, H., Tao, S., Tian, C., Song, S., Jiang, W., Chen, L., et al. (2020). Human exposure to polychlorinated biphenyls embodied in global fish trade. Nat. Food *1*, 292–300.

44. Lian, L., Huang, T., Ke, X., Ling, Z., Jiang, W., Wang, Z., Song, S., Li, J., Zhao, Y., Gao, H., et al. (2022). Globalization-driven industry relocation significantly reduces arctic PAH contamination. Environ. Sci. Technol. *56*, 145–154.

45. Wu, M., Luo, J., Huang, T., Lian, L., Chen, T., Song, S., Wang, Z., Ma, S., Xie, C., Zhao, Y., et al. (2022). Effects of African BaP emission from wildfire biomass burning on regional and global environment and human health. Environ. Int. *162*, 107162.

46. Huang, T., Jiang, W., Ling, Z., Zhao, Y., Gao, H., and Ma, J. (2016). Trend of cancer risk of Chinese inhabitants to dioxins due to changes in dietary patterns: 1980–2009. Sci. Rep. *6*, 21997.

47. van der Veen, I., and de Boer, J. (2012). Phosphorus flame retardants: properties, production, environmental occurrence, toxicity and analysis. Chemosphere *88*, 1119–1153.

48. MacLeod, M., Fraser, A.J., and Mackay, D. (2002). Evaluating and expressing the propagation of uncertainty in chemical fate and bioaccumulation models. Environ. Toxicol. Chem. *21*, 700–709.

49. Shen, H., Huang, Y., Wang, R., Zhu, D., Li, W., Shen, G., Wang, B., Zhang, Y., Chen, Y., Lu, Y., et al. (2013). Global atmospheric emissions of polycyclic aromatic hydrocarbons from 1960 to 2008 and future predictions. Environ. Sci. Technol. *47*, 6415–6424.

50. Hydraulics, D. (2020b). Delft3D-FLOW User Manual (Delft, the Netherlands).

51. Zheng, P., and Chen, X. (2013). Numerical simulation to 3-D structure of water temperature of BS in summer. Period. Ocean Univ. China *43*, 9–16.

52. Wang, Y., Zheng, X., Yu, X., and Liu, X. (2017). Temperature and salinity effects in modeling the trajectory of the 2011 Penglai 19-3 oil spill. Mar. Georesour. Geotechnol. *35*, 946–953.

53. Mackay, D., and Wania, F. (1995). Transport of contaminants to the Arctic: partitioning, processes and models. Sci. Total Environ. *160–161*, 25–38.

54. Wania, F., Axelman, J., and Broman, D. (1998). A review of processes involved in the exchange of persistent organic pollutants across the air–sea interface. Environ. Pollut. *102*, 3–23.

55. Mao, X., Jiang, W., Zhao, P., and Gao, H. (2008). A 3-D numerical study of salinity variations in the BS during the recent years. Continent. Shelf Res. *28*, 2689–2699.

56. Wang, J., Shen, Y., and Guo, Y. (2010). Seasonal circulation and influence factors of the BS: a numerical study based on Lagrangian particle tracking method. Ocean Dynam. *60*, 1581–1596.

57. Qing, S., Zhang, J., Cui, T., and Bao, Y. (2013). Retrieval of sea surface salinity with MERIS and MODIS data in the BS. Remote Sens. Environ. *136*, 117–125.

58. Sun, H., Wu, W., and Wang, L. (2009). Phenanthrene partitioning in sediment-surfactant-fresh/saline water systems. Environ. Pollut. *157*, 2520–2528.

59. Wang, J., Wang, C., Huang, Q., Ding, F., and He, X. (2015). Adsorption of PAHs on the sediments from the yellow river delta as a function of particle size and Salinity. Soil Sediment Contam.: Int. J. *24*, 103–115.

STAR★METHODS

KEY RESOURCES TABLE

REAGENT OR RESOURCE	SOURCE	IDENTIFIER
Sea Meteorological data	NOAA Physical Sciences Laboratory	https://psl.noaa.gov/
Sea Meteorological data	National Marine Date Center	http://www.mds.nmdis.org.cn/
Meteorological data	China Meteorological Administration	http://data.cma.cn/
River discharge	Ministry of Water Resources	http://www.mwr.gov.cn/

RESOURCE AVAILABILITY

Lead contact

Further information and requests should be directed to and will be fulfilled by the lead contact, Dr. Hong Gao (honggao@lzu.edu.cn).

Materials availability

This study did not generate new unique reagents.

Data and code availability

Some publicly available datasets used in this article are listed in the key resources table. The other data associated with model inputs are available as reported in this article and STAR Methods.

This paper does not report original code.

Any additional information required to reanalyze the data reported in this paper is available from the lead contactupon request.

METHOD DETAILS

The Bohai Sea

The BS is a nearly enclosed interior sea with an area of approximately 77,000 km^2, with a length of the coastline of 3,784 km and a mean depth of 18 m, respectively (Figure S8). The BS Rim includes Liaoning, Hebei, Shandong provinces and Tianjin municipality.[3] The seawater in the BS is characterized by low salinity (~30‰), low temperature (0-21°C), low clarity, and high suspended matter contents. Thirty-six major rivers are entering the BS; the total water volume of these 36 rivers accounted for about 96% of all the rivers emptying into the BS. Further information can be found in Table S2 of Supporting Information (SI).[5]

3D-hydrodynamic and emerging contaminant model

Coastal industrial wastewater and sewage from the Bohai Sea Rim region, typically Tianjin, Hebei, Shandong, Liaoning, and other places, have been reported directly discharge chemicals into the BS or the tributary rivers.[5] A 3D-OPFR terrestrial runoff model in the BS integrating hydrodynamic and water quality processes were set up based on Delft3D-FLOW and Delft3D-Water quality (Delft3D-WAQ) modules.[38] The Delft3D-FLOW module was adopted to simulate 3-dimensional unsteady flow, transport (e.g., salinity as a tracer), and water temperature of the BS. The Delft3D-FLOW also provides a hydrodynamic basis for the water quality simulation. The stratification induced by salinity or temperature is considered in this module. The model domain covers the BS and extends from 37°N to 41.05°N and from 117.5°E to 122.5°E with a grid spacing of 3 km (Figure S9). The boundary of the BS area was obtained from the satellite remote sensing image. ArcGIS (10.7, ESRI) was applied to vectorize the terrain, water depth, and boundary and to determine the open and closed BS boundaries. The ArcGIS estimated model domain was transformed into 21158 (142×149, 3 km×3 km) orthogonal curved grids.

The 3D-OPFR model considers five layers in the BS seawaters in the vertical. The advection-diffusion-reaction equations are solved in the 3D Delft3D-WAQ module for OPFR. Delft3D-WAQ provides an option to

input constant atmospheric concentration and deposition, which is often taken from field sampling data, as the model drivers for a targeted substance to be modeled. The temporal and spatial distributions of OPFR on a yearly basis were simulated to identify the transport of OPFR in 36 rivers draining into the BS. The Delft3D-FLOW and Delft3D-WAQ were run during different periods (Table S3). Meteorological data driving these two modules were collected from the websites https://psl.noaa.gov/ and http://data.cma.cn/, respectively. In the study area, the main driving forces of ocean current include gravity, geostrophic deflection force, and tide. Sea temperature and salinity information were taken from the literature (Table S4). The tidal harmonics constants were obtained from the harmonic analysis of 2013 tidal data (K1, O1, P1, Q1, M2, S2, N2, K2). The seawater density is taken as 1024.2 kg/m^3.

Three modeling scenarios were designated to quantify the influence of atmospheric deposition fluxes and air-water exchange fluxes on the input of OPFR to the BS. In the first scenario (Scenario 1), we simulate the terrestrial runoff without taking atmospheric deposition fluxes and air-water exchange fluxes into consideration. Scenario 2 considered a constant atmospheric deposition flux of 2000 ng/m^2/day and atmospheric concentration of 2 ng/m^3, taken from ChnMETOP modeled annual mean values (see next section 2.3), in terrestrial runoff,[16,29] thereby to discern the surface runoff with and without the disturbance from atmospheric deposition and air-water exchange. Scenario 3 considered a constant atmospheric deposition flux of 200 ng/m^2/day and atmospheric concentration of 0.2 ng/m^3 in terrestrial runoff[2,16,29] to further examine the sensitivity of the Delft3D-WAQ simulated OPFR seawater concentration to perturbations from its atmospheric deposition and air-water exchange.

The primary physicochemical properties of OPFRs are presented in Table S5, collected from Estimation Programs Interface Suite (EPI Suite™). The EPI Suite™ is a useful software suite providing estimated physicochemical and environmental fate properties developed by the USEPA and Syracuse Research Corp.[39,40] Other parameters of model associated with OPFR's physicochemical properties are presented in Table S6.

Atmospheric transport model

Chinese Model for Environmental Transport of Organic Pollutants (ChnMETOP) was developed based on the Canadian Model for Environmental Transport of Organochlorine Pesticides. The ChnMETOP is a coupled atmospheric transport, deposition, and multimedia exchange model that has been extensively employed to quantify source-receptor relationships, multi-environmental cycling, and health risks of POPs from regional and global perspectives.[41–45] ChnMETOP is a three-dimensional atmospheric transport model based on the atmospheric advection-diffusion equation, which includes the main dynamics and thermodynamic processes in the atmosphere and the atmospheric boundary layer process.[41,43,46]

The ChnMETOP model domain covers the entire China. The model integration was performed for 2013 on a 0.25°×0.25° latitude/longitude spacing using a recently developed gridded emission inventory of OPFRs in China on the same spatial resolution as the ChnMETOP (Figure S3).[2] The model was integrated from December 1st, 2012, to December 31st, 2013, with December 2012 as the model spin-up time to reach an equilibrium status of OPFR concentrations between the seawater and the air. The major air-water exchange processes include diffusive net gas exchange and dry and wet deposition. The positive flux is referred to as the upward transfer of OPFRs from the water to air or volatilization, and the negative as the downward transfer or diffusive gaseous deposition. Meteorological data (e.g., wind, atmospheric pressure, temperature, and precipitation) driving the ChnMETOP used the 6-hourly objectively analyzed data from the National Centers for Environmental Prediction (NECP) and the Final Operational Global Analysis (http://dss.ucar.edu/datasets/ds083.2/) on a spatial resolution of 1°×1° latitude/longitude. The meteorological data were then interpolated into ChnMETOP model grids (0.25°×0.25° latitude/longitude) and a time step length of 20 min. Detailed model descriptions and evaluations and chemical/physical properties of OPFRs can be found in our previous study.[2]

Loading estimation

Two-film model was used to calculate the air-water diffusive gaseous exchange flux (F_{aw}, ng/m^2/day) of organophosphorus flame retardants (OPFRs),[29] defined by

$$F_{aw} = k_{ol}(C_w - C_aRT/H) \quad \text{(Equation 1)}$$

where k_{ol} is the overall mass transfer coefficient (m/day), C_a and C_w are the concentration of OPFRs in air (ng/m^3) and dissolved water (ng/m^3), respectively, H is the Henry's Law Constant,[7,47] T is the temperature (K) and R is the gas constant (8.314 Pa m^3/mol/K).

Uncertainty and sensitivity analysis of atmospheric deposition

The ChnMETOP (Chinese Model for Environmental Transport of Organic Pollutants) model includes complex dynamical and physical processes, such as deposition and precipitation scavenging, horizontal and vertical advection, turbulent diffusion, and exchange between environmental media. It is impossible to examine the uncertainties in each physical and dynamic processes. Instead, we used a first-order error propagation approach to evaluate the uncertainties in modeled seawater concentrations (Cf_{out}) of OPFR.[43] In this method, uncertainties were calculated by propagating input parameter (Cf_i) uncertainties defined by[48]

$$Cf_{out} = exp\sqrt{\sum_i (lnCf_i)^2 \times S_i^2}, \quad \text{(Equation 2)}$$

where Cf_{out} and Cf_i are the confidence factors that span the 95% confidence interval around the median of a log-normally distributed variable, and S_i is the relative sensitivity of the model output subject to changes in input parameter i. The relationships between Cf and standard deviation (σ) of a log-normal distribution are

$$Cf = e^{2\sigma}. \quad \text{(Equation 3)}$$

The coefficient of variation CV is given by

$$CV = \sqrt{e^{\sigma^2} - 1}, \quad \text{(Equation 4)}$$

where CV is defined as the ratio of the standard deviation to the mean.

The sensitivity (S) is calculated by

$$S = \left(\Delta O/O\right) \Big/ \left(\Delta I/I\right), \quad \text{(Equation 5)}$$

where ΔI and ΔO are the relative changes in input (I) and output (O) parameters of interest, respectively.

Considering that OPFRs have a broad range of physicochemical properties, we test the sensitivities of model input and output variables to the changes in major physicochemical properties using Equation 5. We also considered other model parameters that significantly affect OPFR emissions and modeling results.[2] The average sensitivity of increasing and decreasing input parameter was calculated. Each input parameter was altered individually by $\pm$10%, respectively.[49] Uncertainties and sensitivities of the OPFR physicochemical properties defined by Cf (Equation 3) and S (Equation 5) values are presented in Table S7. In the Delft3D-WAQ modeling, we took different physicochemical properties in 11 major OPFR congeners into account. Details are presented in Table S6. We estimated an overall uncertainty of OPFR emissions and seawater concentration at 2.81 and 1.25 in 2013, respectively. The estimated the sensitivity of wind speed and temperature is 1.28 and 1.21 for air-water diffusive gaseous exchange flux.

Validation of 3D-hydrodynamic model

The fate of POPs depends on many processes in the marine environment. Since these processes include, for example, advection and mixing, and can be strongly affected by physical properties of water, such as temperature, a hydrodynamic model is a prerequisite tool for conducting model investigations.[50] The model is validated by comparing modeled surface temperature and salinity with available observational data. Figure S10 shows Delft3D-FLOW simulated sea surface temperatures (SST) across the BS in 2013. Relatively higher SSTs can be seen in Liaodong Bay, Bohai Bay, and Laizhou Bay. In contrast, lower SSTs can be identified in the Bohai Strait in June and September, respectively. High-temperature tongues extended from each of the three bays to the center. In March and December, however, we observe opposite SST spatial pattern. Our results are in line, to a large extent, with previous research results,[51,52] demonstrating that the model is capable of reproducing temporal-spatial variations of SST across the BS. The temperature/climate dependence of air–sea exchange is important decisive factor in the global distribution of POPs. Persistent chemicals are transported from the areas with net evaporation to the areas of net deposition. The direction of net flux is often controlled by temperature.[53] The impact of temperature

on air-water exchange is complex and manifold. The main processes contributing to the air-water exchange of POPs are diffusive vapour exchange, precipitation scavenging of vapours and particle-sorbed chemicals, and particle dry deposition. The relative importance of these processes is mostly dependent on a chemical's specific properties (volatility, hydrophobicity, etc.).[54]

Sea surface salinity (SSS) plume distribution is shown in Figure S3. The salinity is relatively low in those areas with freshwater runoff input, especially in the estuaries of the Yellow River and Liaohe River with relatively strong runoff. Salinity, as a passive tracer, represents the advection-dispersion of contaminants under subject to the influence of the flow pattern. By comparing the horizontal distribution of the salinity field in winter and summer, it can be found that the salinity in winter is slightly higher than that in summer, especially in the waters near the mouth of the Yellow River and the Liaohe River. Lower salinity in summer can be attributed to higher precipitation, which input more freshwater into seawaters and rivers emptying into the BS. Overall, salinity in different months/seasons illustrates identical spatial distribution pattern with higher values in the boundaries with the Yellow Sea.[55–57] High salinity can improve the adsorption capacity of POCs by water, clay, and sediments in the BS.[58,59]

The hydrodynamic model was validated by comparing modeled SST and SSS with available field measurements collected from data portal (https://psl.noaa.gov/, SSS), and Advanced Very High Resolution Radiometer (AVHRR, for SST) in 2013. The results are presented in Figure S4. In general, the modeled SST (Figure S4A) and SSS (Figure S4B) match well with that measured at the sampling sites S1 - S6 (Figure S9), indicating the model performed well. The correlation coefficients between modeled and measured SST and SSS reached $R^2 = 0.88$ ($n = 72$, $P < 0.01$) and $R^2 = 0.79$ ($n = 72$, $P < 0.01$), respectively (Figure S4). Since salinity acts primarily as a passive tracer and thus largely reflects current seawater characteristics, we can consider that the model responds well to the forcing at the water surface and the open boundary, implying that the advection and diffusion across the BS seawaters are reasonably simulated.